PNAS
www.pnas.org

Supporting Information for

Volatile loss following cooling and accretion of the Moon revealed by chromium isotopes

Paolo A. Sossi[a*], Frédéric Moynier[a, b], Kirsten van Zuilen[a,^]

[a] Institut de Physique du Globe de Paris, Université Paris Diderot, Université Sorbonne Paris Cité, CNRS UMR 7154, 1 rue Jussieu, 75238 Paris Cedex 05, France

[b] Institut Universitaire de France, Paris, France

[^]Present address: Department of Earth Sciences, Vrije Universiteit Amsterdam, 1081 HV Amsterdam, The Netherlands

* Corresponding author: sossi@ipgp.fr

This PDF file includes:

Supporting Information Text

Sample selection and description

Komatiite samples were chosen to characterise the chromium isotope composition of the bulk silicate Earth for several reasons; *i)* they are the products of high degrees of melting (≥25 % (1)) of the mantle and *ii)* these high degrees of melting, coupled with high pressures, require mantle potential temperatures in excess of ambient mantle (2). As the magnitude of equilibrium mass-dependent isotopic fractionation is proportional to $1/T^2$ (3), both of these features act to dampen the extent of isotopic fractionation between the melt and the source of the komatiites (4). These sources themselves are often near-primitive, having experienced ≤5% prior melt extraction, offering little scope for isotopic disturbance and thereby reflecting that of the primitive mantle. Komatiites have been used successfully in a variety of stable isotopic studies to assess the composition of the bulk silicate earth (5–8). Furthermore, when coupled with modern peridotites, komatiites also afford the opportunity of assessing temporal variations in the Cr isotopic composition of Earth's mantle. This analysis is complementary to that based on evidence from igneous rocks that the Cr abundance of the mantle has remained constant to at least 3.9 Ga (9).

Komatiite samples showing an olivine spinifex texture of the order of mm to cm, coming from the upper, A1 and A2 zones of komatiite flows, were preferentially selected for this study. This is because these samples are more likely to represent quenched liquids (10–12) than do samples from other zones in komatiite flows (A3 and B zones), which crystallised under a thermal gradient and accumulated olivine, respectively (13). The komatiites come from five cratons, comprising the 3.48 Ga Komati formation of the Barberton Greenstone Belt, Kaapvaal craton (49J, 331/783, 331/777A, 331/790, 331/779); 2.7 Ga Reliance formation of the Belingwe Greenstone Belt, Zimbabwe craton (B-R1); the 3.515 Ga Coonterunah (179/751) and 3.2 Ga Regal formation (176/723) of the Pilbara craton; the 2.7 Ga Scotia (SD5/354.5; SD6/400) and Marshall Pool (331/948) groups of the Yilgarn craton; and the 2.7 Ga Pyke Hill locality of the Munro Township, Abitibi Belt, (422/84, 422/94, 422/95, 422/96) and the Red Lake greenstone belt (RL-12-1 (14)), Superior Craton. They include a combination of both aluminium-depleted and –undepleted types. The reader is referred to refs. (4, 12) for in-depth petrographic, geochemical and petrologic descriptions of these samples.

The lunar samples reflect a wide range of igneous rocks, with the purpose of gaining a representative cross-section of the composition of the lunar mantle, which is known to be heterogeneous mineralogically (15, 16). As such mineralogical variation has been shown to induce stable isotopic fractionation (for example, iron in lunar mare basalts (17)), it is important to assess whether the Cr

isotope composition of the Moon can be satisfactorily determined with extant lunar return samples. In view of minimising possible isotopic fractionation induced by a lunar magma ocean (see refs. (18, 19) for examples with Fe), samples from the cumulate Mg Suite were selected. These samples are a set of consanguineous rocks that now have metamorphic textures (20) and are typified by their high Mg#s and anorthite contents in plagioclase, coupled with depletions in compatible elements, and, in some cases, enrichment in incompatible trace elements typical of KREEP (potassium-rare-earth-element-phosphorus) (21, 22). These features are interpreted to reflect *i)* their primitive, largely olivine-bearing source that must have been among the first to crystallise from a lunar magma ocean (23), as reflected in their ≈4.4 Ga ages, one of the oldest products of lunar magmatism and *ii)* the precipitation of metallic iron, likely during the ascent of their parent magma (19, 24). As such, they are able to provide insights into the initial stages of lunar formation, prior to the formation of the lunar mare basalts. Furthermore, as they are likely cogenetic (21), their magmatic evolution may be interpreted together using crystal-liquid equilibria constraints, allowing the effect of magmatic differentiation to be quantified.

The samples studied include a dunite (72415), a troctolite (76535), and four norites (78238, 78235, 15445 and 15455). Mare basalts of both the High Ti- (10003, 10057, 70135) and Low Ti groups (12002, 15555) were selected, in order to assess the impact of differing source regions on the isotope composition of chromium. In addition, the lunar green glass (15426) was also analysed, due to its distinct composition in terms of volatile elements and its high Mg# and therefore primitive source region (25, 26). The deposition of sublimates of volatile metals (including Fe and Cr) may also cause fractionation in its isotopic composition (see discussion in ref. (19)). Further information on these samples is provided in the lunar sample compendium (https://curator.jsc.nasa.gov/lunar/lsc/index.cfm), and refs. (19) and (21) and references therein.

Modelling Cr isotope evolution in the lunar Mg Suite

The Mg Suite samples are phaneritic, cumulate rocks that now possess metamorphic textures (20). Their bulk composition is a reflection of that of their constituent minerals, facilitating calculation of mineral modes by least-squares chi-squared minimisation:

$$\chi^2 = \sum_i \left(\sum_n f_n X_n^i - X_{WR}^i\right)^2 \text{ (S1)}$$

Where X^i is the concentration of the ith oxide in the nth phase or whole rock (WR), where the sum is performed over all major oxides (i); SiO_2, Al_2O_3, FeO, MgO and CaO. Mineral compositions come from refs. (27, 28). Calculated mineral modes, compositions and χ^2 values are given in Table S1.

Table S1. Whole rock and mineral compositions, and mineral modes calculated by least-squares chi-squared minimisation for Mg Suite cumulates analysed in this work.

	SiO_2 (wt. %)	Al_2O_3 (wt. %)	FeO (wt. %)	MgO (wt. %)	CaO (wt. %)	Cr (ppm)	Mode
72415							
Ol	40.24	0	12.29	46.65	0.13	274	0.94
Opx	54.13	0.96	6.94	32.59	2.24	1505	0.01
Plg	44.79	35	0	0	19.25		0.05
Chr						342105	0.006
WR	39.93	1.53	11.34	43.61	1.14		
WR Calc	40.67	1.92	11.57	43.99	1.20	2325	
Difference	-0.74	-0.39	-0.23	-0.38	-0.06		
χ^2							**0.90**
76535							
Ol	40.3	0	12.29	46.65	0.03	137	0.39
Opx	55.89	1.26	7.55	32.23	1.44	5474	0.03
Plg	44.21	35.89	0	0	19.6		0.58
Chr						342105	0.002
WR	42.88	20.73	4.99	19.09	11.41		
WR Calc.	42.97	20.86	5.03	19.20	11.42	709	
Diff.	-0.09	-0.13	-0.04	-0.11	-0.01		
χ^2							**0.04**
78238/5							
Opx	55.08	1.08	12.17	29.65	1.47	0.63	0.41
Plg	44.79	34.79	0	0	19.09		0.59
WR	49.50	20.87	5.05	11.76	11.71		
WR Calc.	49.01	20.98	4.99	12.15	11.87	1766	
Diff.	0.49	-0.11	0.06	-0.39	-0.16		
χ^2							**0.44**
15445							
Opx	55.08	1.08	12.17	29.65	1.47	0.63	0.37
Plg	44.79	34.79	0	0	19.09		0.63
WR	49.44	21.90	3.85	10.20	12.80		
WR Calc.	48.55	22.47	4.45	10.83	12.65	1575	
Diff.	0.89	-0.57	-0.60	-0.63	0.15		
χ^2							**1.91**
15455							
Opx	55.08	1.08	12.17	29.65	1.47	0.5	0.24
Plg	44.79	34.79	0	0	19.09		0.76
WR	47.7	27	2.7	6.96	14.8		
WR Calc.	47.22	26.83		7.00	14.93	808	
Diff.	0.48	0.17		-0.04	-0.13		
χ^2							**0.28**

A model is also presented in which a parent magma (19, 20) with 13 wt. % MgO, 10 wt. % FeO, 2300 ppm Cr, and $\delta^{53}Cr$ = -0.24 ‰ undergoes fractional crystallization at fractions (*f*) of 0.05. The oxygen fugacity is set to IW-1 ($\log fO_2$ = -10.71 at 1300°C), and the resulting $Cr^{2+}/\sum Cr$ ratio in the magma is calculated as:

$$\frac{Cr^{2+}}{\sum Cr} = \frac{1}{\left(1+10^{\left(\frac{1}{4}\log fO_2+\log K\right)}\right)}, \text{(S2)}$$

where $\log K$ = 1.9 (29), giving $Cr^{2+}/\sum Cr$ = 0.86. Temperature at 1 bar, anhydrous, is calculated according to the relation (12):

$$T^oC\ (1\ bar) = 1091 + 16 \times MgO\ (wt.\%) \text{ (S3)}$$

Yielding 1299 °C for the parent magma. The partitioning of Fe and Mg between olivine and orthopyroxene and the melt is governed by the equation (30):

$$K_{D\ Fe-Mg}^{Ol,Opx-Melt} = \frac{\left(\frac{XFe}{XMg}\right)_{Ol,Opx}}{\left(\frac{XFe}{XMg}\right)_{Melt}} = 0.30. \text{ (S4)}$$

Partition coefficients for Cr^{2+} and Cr^{3+} between olivine (31), orthopyroxene (32) and melt are:

$$D_{Cr}^{Ol-Melt} = 0.66\left(\frac{10^4}{T(K)}\right) - 4.48 \text{ (S5)}$$

$$D_{Cr^{2+}}^{Opx-Melt} = -0.0045 \times T(K) + 7.70 \text{ (S6)}$$

$$D_{Cr^{3+}}^{Opx-Melt} = -0.0561 \times T(K) + 94.6 \text{ (S7)}$$

Chromite was assumed to contain 50 wt. % Cr_2O_3.

The $^{53}Cr/^{52}Cr$ fractionation factor is given by the following equation (33), which accounts for the different $Cr^{2+}/\sum Cr$ ratios between two phases, A and B:

$$\Delta^{53}Cr_{A-B} = 0.35 \times \left(\left(\frac{Cr^{2+}}{\sum Cr}\right)_B - \left(\frac{Cr^{2+}}{\sum Cr}\right)_A\right) \times \frac{10^6}{T^2}. \text{ (S8)}$$

Output results for each phase in the model are shown in Tables S2-S7.

Table S2: Melt

F	T	P	MgO (wt %)	FeO (wt %)	Mg#	Cr^{2+}	Cr^{3+}	Cr	$\Delta 53Cr_{Min\text{-}Melt}$	$\delta^{53}Cr_{Melt}$
0	1299		13.0	10.0	0.699	1971	329	2300	-0.01	-0.24
0.05	1271		11.3	9.9	0.669	1987	332	2319	-0.01	-0.24
0.1	1256		10.3	10.1	0.646	2031	339	2369	-0.01	-0.24
0.15	1241		9.4	10.2	0.620	2081	347	2428	-0.01	-0.24
0.2	1231		8.7	10.5	0.598	2155	360	2515	-0.01	-0.24
0.25	1219		8.0	10.7	0.571	2231	372	2604	-0.01	-0.24
0.3	1197		6.6	10.7	0.525	2277	380	2657	0.03	-0.25
0.35	1184		5.8	11.0	0.485	2379	128	2507	0.07	-0.26
0.4	1176		5.3	11.6	0.450	2519	41	2560	0.10	-0.28
0.45	1173		5.2	11.7	0.441	2594	42	2636	0.13	-0.31

Table S3: Olivine

F	T	P	MgO (wt %)	FeO (wt %)	Mg#	Cr^{2+}	Cr^{3+}	Cr	$\Delta^{53}Cr_{Ol\text{-}Melt}$
0	1299	1	48.3	11.1	0.886	1659	277	1936	-0.02
0.05	1271	0.75	47.2	12.4	0.871	1901	317	2218	-0.02
0.1	1256	0.65	46.3	13.6	0.859	2082	347	2429	-0.02
0.15	1241	0.55	45.3	14.8	0.845	2271	379	2650	-0.02
0.2	1231	0.5	44.3	15.9	0.832	2451	409	2860	-0.02
0.25	1219	0.5	43.2	17.3	0.816	2658	444	3101	-0.02
0.3	1197	0.25	41.2	19.8	0.787	2943	491	3435	-0.02

Table S4: Orthopyroxene

F	T	P	MgO (wt %)	FeO (wt %)	Mg#	Cr^{2+}	Cr^{3+}	Cr	$\Delta^{53}Cr_{Opx\text{-}Melt}$
0.3	1197	0.24	29.6	13.9	0.791	2163	3040	5204	0.11
0.35	1184	0.5	28.3	15.6	0.763	2363	1087	3450	0.06
0.4	1176	0.5	27.1	17.2	0.737	2623	332	2955	0.02
0.45	1173	0.5	26.8	17.7	0.730	2817	28	2845	0.01

Table S5: Plagioclase

F	T	P
0.05	1271	0.25
0.1	1256	0.35
0.15	1241	0.45
0.2	1231	0.5
0.25	1219	0.5
0.3	1197	0.5
0.35	1184	0.5
0.4	1176	0.5
0.45	1173	0.5

Table S6: Chromite

F	T	P	MgO (wt %)	FeO (wt %)	Mg#	Cr^{2+}	Cr^{3+}	Cr	$\Delta^{53}Cr_{Chr\text{-}Melt}$
0.3	1197	0.001				0	342105	342105	0.19
0.35	1184	0.0005				0	342105	342105	0.19
0.4	1176	0.0005				0	342105	342105	0.19
0.45	1173	0.0003				0	342105	342105	0.19

Table S7: Instantaneous Cumulate

F	T	P	MgO (wt %)	FeO (wt %)	Mg#	Cr^{2+}	Cr^{3+}	Cr	$\Delta^{53}Cr_{Min\text{-}Melt}$	$\delta^{53}Cr_{\ cumulate}$
0	1299		48.3	11.1	0.886	1659	277	1936	-0.01	-0.26
0.05	1271		35.4	9.3	0.871	1426	238	1664	-0.01	-0.26
0.1	1256		30.1	8.8	0.859	1353	226	1579	-0.01	-0.26
0.15	1241		24.9	8.1	0.845	1249	209	1458	-0.01	-0.26
0.2	1231		22.2	8.0	0.832	1225	205	1430	-0.01	-0.26
0.25	1219		21.6	8.7	0.816	1329	222	1551	-0.01	-0.26
0.3	1197		17.4	8.3	0.789	1282	1213	2495	0.03	-0.18
0.35	1184		14.1	7.8	0.763	1237	648	1886	0.07	-0.17
0.4	1176		13.5	8.6	0.737	1311	337	1648	0.10	-0.16
0.45	1173		13.3	8.8	0.730	1408	117	1525	0.13	-0.13

The compositions of the highlands Mg Suite cumulates are then made from combinations of olivine, orthopyroxene, plagioclase and chromite that crystallised in the model.

Table S8: Re-constructed compositions of Mg Suite cumulates from the crystallisation model.

	MgO (wt. %)	FeO (wt. %)	Cr (ppm)	δ^{53}Cr
72415				
95% Olivine	47.2	12.4	2219	-0.26
5% Plagioclase	0	0	0	
Whole Rock	44.8	11.8	2108	-0.26
76535				
39% Olivine	47.2	12.4	2219	-0.27
61% Plagioclase	0	0	0	
Whole Rock	18.4	4.9	865	-0.27
78238/5				
40% Orthopyroxene	29.6	13.9	3450	-0.14
60% Plagioclase	0	0	0	
Whole Rock	11.84	5.57	1380	-0.14
15455				
25% Orthopyroxene	28.3	15.6	3450	-0.14
75% Plagioclase	0	0	0	
Whole Rock	7.4	4.1	897	-0.14
15445				
15455 WR	7.4	4.1	8.97	-0.14
+.25% Chromite			342105	-0.06
Whole Rock	7.1	3.90	1579	-0.10

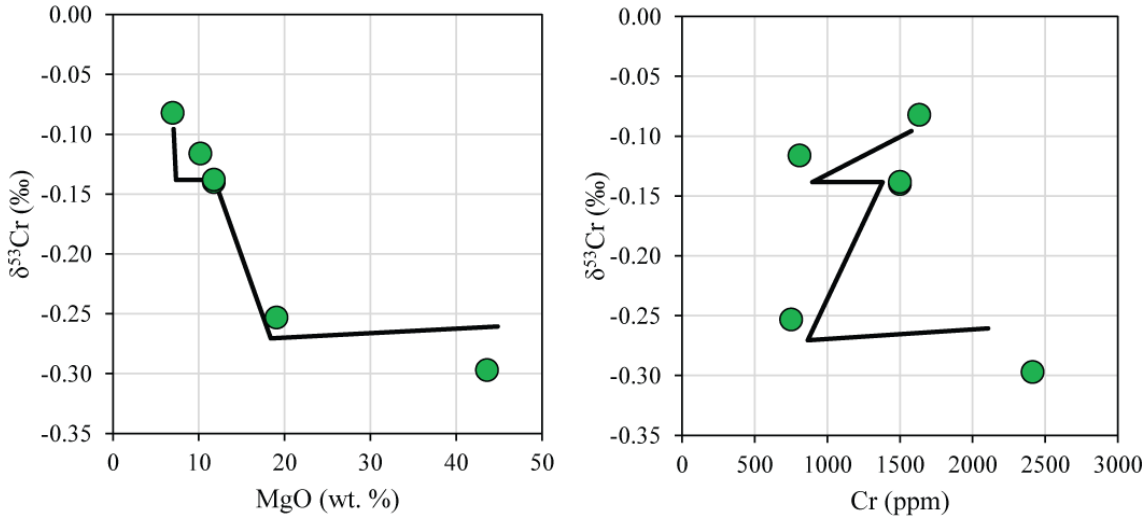

Figure S1. Variation of δ^{53}Cr (‰) against a) MgO (wt. %) and b) Cr (ppm), as measured (green circles) and modelled (black lines).

Assessment of the composition of the Earth's mantle and the Moon

Bulk Silicate Earth (BSE)

Previous estimates of the BSE included rocks that were not representative of Earth's mantle (*e.g.*, wherlites, amphibolites; (34, 35)) and, based on the mechanisms presented above, may have therefore experienced prior Cr isotope fractionation following extraction of their precursor magma from the mantle. Furthermore, many peridotites used in these former studies experienced varying degrees of depletion, which may equally have altered their Cr isotope composition relative to primitive mantle. A compilation of literature data for peridotites that are fertile, unmetasomatised with Cr contents of 2520±630 ppm, Mg# (molar Mg/(Mg+Fe)) between 0.885 and 0.910, and >2 wt. % Al_2O_3; along with spinifex-texture komatiites (from this study) is presented in Table S9.

Table S9: Compilation of Cr isotope data for terrestrial ultramafic rocks.

Locality	Sample Name	δ^{53}Cr (‰ *vs.* SRM-979)	±2SD	Cr (ppm)	Mg#	Grubb's Test
Xia et al., 2017						
Shavaryn	Sh11-1x	-0.08	0.05	2532	0.891	
	Sh11-4x	-0.22	0.05	2737	0.896	x
	Sh11-15x	-0.20	0.04	2600	0.898	x
	Sh11-22x	0.06	0.05	2600	0.909	x
	Sh11-48x	-0.13	0.04	2599	0.895	
	Sh11-58x	-0.16	0.04	2736	0.899	
	Sh11-59x	0.05	0.04	2258	0.901	x
	Sh11-65x	-0.10	0.04	2326	0.894	
	4230-15Lhz	-0.09	0.04	1984	0.904	
Haer	H11-1	-0.24	0.04	2462	0.898	x
	H11-3	-0.05	0.04	2531	0.888	
	H11-10	-0.17	0.05	2668	0.905	
	H11-14	-0.13	0.04	2531	0.893	
Udachnya	U-85	-0.10	0.04	2846	0.896	
Hannuoba	DMP04	-0.12	0.04	2477	0.911	
	DMP41	-0.07	0.04	2736	0.902	
	DMP58	-0.11	0.04	2326	0.897	
	DMP60	-0.21	0.04	2668	0.899	x
Schoenberg et al., 2008						
Val Moleno Lherzolite	CH70-5	-0.125	0.048	2103		
Harz Mtns	GZG1275/4	-0.111	0.048	2274		
Schoenberg et al., 2016						
Finero Lherzolite	MIH-Per1	-0.071	0.048	2273		

Harz Mtns	GZG1275/4	-0.143	0.048	2639		
Sossi et al. this work						
Komati Fm, Barberton	49J	-0.065	0.041	3190	0.839	
Reliance Fm, Belingwe	B-R1	-0.155	0.035	2650	0.824	
Coonterunah Fm, E. Pilbara	179-751	-0.122	0.066	3240	0.797	
Regal Fm., W. Pilbara	176-723	-0.122	0.048	2450	0.869	
Scotia, Yilgarn	SD5-354.5	-0.121	0.017	3050	0.806	
Komati Fm., Barberton	331/783	-0.082	0.039	2894	0.797	
Komati Fm., Barberton	331-777A	-0.114	0.012	2717	0.794	
Munro, Superior	422-94	-0.147	0.035	3464	0.788	
Munro, Superior	422-95	-0.168	0.059	3260	0.794	
Munro, Superior	422-84	-0.112	0.004	2902	0.854	
Red Lake, Superior	RL-12-1	-0.111	0.010	1351	0.692	
Komati Fm., Barberton	331/790	-0.132	0.006	3371	0.799	
Munro, Superior	422/96	-0.097	0.001	3060	0.867	
Scotia, Yilgarn	SD6/400	-0.098	0.004	2428	0.828	
Munro, Superior	422/96a	-0.085	0.001	3060	0.867	
Marshall Pool, Yilgarn	331/948	-0.104	0.004	2915	0.753	
Komati Fm., Barberton	331/779	-0.097	0.004	2706	0.820	
Dunite, Twin Sisters	DTS-1	-0.127	0.007	3990	0.919	
Peridotite, Cazadero	PCC-1	-0.083	0.004	2730	0.912	
Dunite, Twin Sisters	DTS-1a	-0.123	0.003	3990	0.919	
		δ^{53}Cr	**±2SD**	**±2SE**		***n***
Average Earth mantle		**-0.114**	**0.056**	**0.040**		**42**
Average Earth mantle (outliers excluded)		**-0.112**	**0.029**	**0.020**		**36**

The Anderson-Darling test for normality on the above dataset after filtering has a D value of 0.184, which is smaller than the critical value, *c* of 0.734 (at a confidence level of 0.05). This attests that the data for the BSE is normally distributed and the 2SE value can be used as an uncertainty of the mean value.

Moon

In a study of the Cr isotope composition of lunar mare basalts, Bonnand and co-workers (36) found a systematic effect of magmatic differentiation on the δ^{53}Cr values. Partially cumulate magmas were found to be isotopically heavy (up to ≈ -0.15‰), whereas magmas that had experienced crystal fractionation of chromite and/or pyroxene tended to be isotopically light (down to ≈-0.30‰). These authors found the data could be fit by a $\Delta^{53}Cr_{min\text{-}melt}$ fractionation factor = -0.15 ‰, consistent with the *ab-initio* calculations (33). In order to minimise the potential effect of chromite and pyroxene precipitation in skewing the database of lunar mare basalts used to calculate the Cr isotope composition of the lunar mantle, petrologic filtering was undertaken (see main text).

Table S10. Petrology, geochemistry and K_D^{Fe-Mg} modelling of lunar mare basalts.

Sample		Cr (ppm)	MgO (wt. %)	FeO (wt. %)	Mg# WR	Mg# Ol/*Px*	Mg# Melt Predict[1]	MgO Predict[1]	FeO Predict[1]	Mg# melt calc[2]	*f*Ol/px
Low Ti											
12002	Ol suite.	5949	14.88	21.66	0.551	0.76	0.49	11.5	21.6	0.49	0.12
12016	**Ilm suite. Primitive olivine basalt, resorbed Ol.**	**3680**	**12.65**	**22.64**	**0.499**	**0.72**	**0.44**	**9.7**	**22.3**	**0.44**	**0.10**
12040	Ol suite. Olivine + chromite cumulate.	3650	16.1	20.9	0.579	0.72	0.44	8.5	19.2	0.44	0.27
12051	Ilm suite. Evolved basalt (no ol except minor fayalite), no cumulus phases (37)	1720	6.4	20.19	0.361	*0.68*	0.39	6.4	20.2	0.36	0.00
12052	**Pig suite. Variolitic, px-phyric, (38) report Fo_{71}.**	**2990**	**8.14**	**19.82**	**0.423**	***0.71***	**0.42**	**8.1**	**19.8**	**0.42**	**0.00**
12064	Pig suite. Evolved px-bearing mare basalt, tr. fayalite only. Kushiro 1971.	1950	6.6	19.83	0.372	*0.65*	0.36	6.6	19.8	0.37	0.00
14053	Al suite. Very low fO_2 (39), ophitic texture, Mg Ol incl. in pig., Fo_{63}.	2874	8.97	16.97	0.485	*0.69*	0.40	5.8	15.6	0.40	0.11
15016	Ol suite. Vesicular - parent magma?; accumulated chr.	6080	11.14	22.58	0.468	0.70	0.41	8.7	22.1	0.41	0.09
15386	**KREEP basalt.**	**2040**	**8.19**	**10.60**	**0.579**						
15555	**Poikilitic plag - same mineralogy as 15016 - parent magma (40)**	**4280**	**11.16**	**22.75**	**0.467**	**0.70**	**0.41**	**8.8**	**22.3**	**0.41**	**0.09**
High Ti											
10003	Evolved basalt.	1583	7.1	20.51	0.382	0.64	0.35	7.1	20.5	0.38	0.00
10017	**No olivine, no evidence for accumulation (41)**	**2330**	**7.72**	**19.49**	**0.414**	***0.73***	**0.45**	**7.7**	**19.5**	**0.41**	**0.00**
10050	**Minor olivine (1%), subophitic texture**	**2250**	**7.86**	**19.29**	**0.421**	**0.68**	**0.39**	**6.8**	**18.9**	**0.39**	**0.04**
10057		**2190**	**7.93**	**19.24**	**0.424**	**0.69**	**0.40**	**7.1**	**19.0**	**0.40**	**0.03**
10058	Evolved basalt, no Ol (resorbed?), no chr., subophitic basalt. (42)	1410	6.11	19.60	0.357	0.65	0.36	6.1	19.6	0.36	0.00
10072	Similar to 10017 except slightly less ilm and more plg (2%)	2390	7.87	19.76	0.415	0.69	0.40	7.5	19.6	0.40	0.01
70017	**Slowly-cooled. Highest Fo_{69}; highest En_{75}**	**3700**	**9.64**	**18.32**	**0.484**	***0.75***	**0.47**	**9.6**	**18.3**	**0.48**	**0.00**
70035		**3530**	**9.89**	**18.50**	**0.488**	***0.75***	**0.47**	**9.9**	**18.5**	**0.49**	**0.00**
70135	**3% ol**	**3921**						**unknown**			
70215	**7% ol, quenched liquid (fine-grained)**	**2680**	**8.52**	**19.62**	**0.436**	**0.75**	**0.47**	**8.5**	**19.6**	**0.44**	**0.00**
74275	**13 % olivine. Dunite xenoliths with Fo84. Highest olivine phenocryst is Fo_{80}**	**3830**	**10.26**	**18.25**	**0.501**	**0.8**	**0.55**	**10.3**	**18.3**	**0.50**	**0.00**
75055	**No olivine.**	**1847**	**6.84**	**18.24**	**0.401**	**0.73**	**0.45**	**6.8**	**18.2**	**0.40**	**0.00**

[1] Mg#, MgO or FeO content of the melt predicted by $K_D^{Fe-Mg} = 0.3$ from Ol or Px composition. [2] Mg# of the melt calculated after *f*Ol/px subtraction. Samples in **bold** meet selection criteria.

Table S11. Chromium isotope compositions of representative lunar samples.

Sample	δ^{53}Cr (‰)	± (2SD)
12016	-0.222	0.022
12052	-0.191	0.022
14053	-0.238	0.022
15386	-0.158	0.022
15555	-0.203	0.022
10017	-0.216	0.022
10050	-0.263	0.022
10057	-0.211	0.022
10057	-0.243	0.002
70017	-0.178	0.022
70035	-0.257	0.022
70135	-0.196	0.012
70215	-0.218	0.022
74275	-0.227	0.022
75055	-0.171	0.022
76535	-0.253	0.005
15426	-0.186	0.009
Average Moon	**-0.212**	**0.064**

The Anderson-Darling test for normality on the lunar dataset has a D value of 0.150, which is smaller than the critical value, *c* of 0.714 (at a confidence level of 0.05). This attests that the data for the BSE is normally distributed and the 2SE value (0.033 ‰) can be used as an uncertainty of the mean value.

Calculation of relative abundances of Cr-bearing gas species

The relative abundance of Cr-bearing gas species is calculated using three homogeneous equilibria:

$$Cr + \frac{1}{2}O_2 = CrO. \text{ (S9)}$$

$$CrO + \frac{1}{2}O_2 = CrO_2. \text{ (S10)}$$

$$CrO_2 + \frac{1}{2}O_2 = CrO_3. \text{ (S11)}$$

The equilibrium partial pressures were calculated using thermodynamic data from the JANAF tables (43).

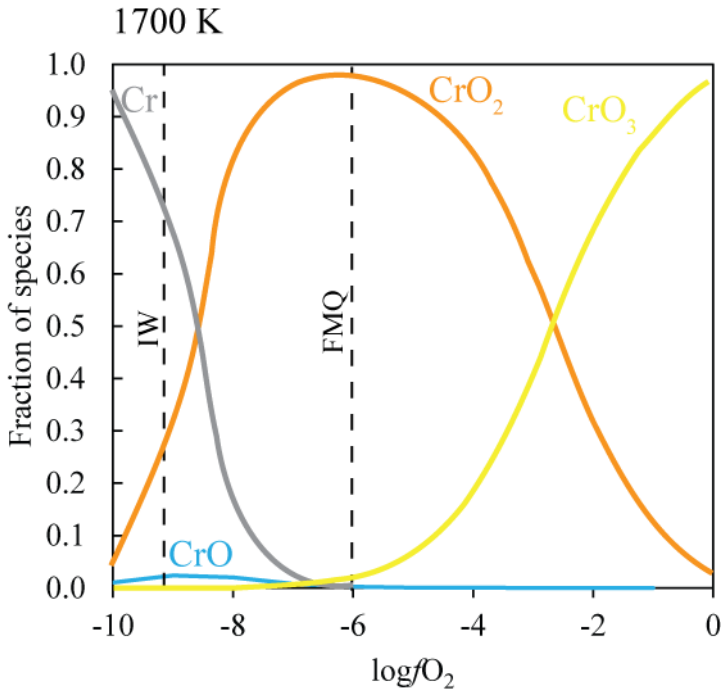

Figure S2. Relative abundances of Cr-bearing gas species at 1700 K, 1 bar assuming an ideal gas as calculated from thermodynamic data of (43).

Calculation of Cr isotope fractionation factors of Cr-bearing gas species

In the simple approximation that vibrational frequencies, which are most affected by isotopic substitutions, are harmonic, the vibrational partition function for a diatomic molecule (here, ^{53}Cr and ^{52}Cr in CrO(g)), can be written (44):

$$\alpha_{CrO(g)-Cr(g)} = \frac{v_{^{53}Cr^{16}O}}{v_{^{52}Cr^{16}O}} \times \left(\frac{\exp\left[-\frac{h v_{^{53}Cr^{16}O}}{2k_B T}\right]}{1-\exp\left[-\frac{h v_{^{53}Cr^{16}O}}{k_B T}\right]} \right) \times \left(\frac{1-\exp\left[-\frac{h v_{^{52}Cr^{16}O}}{k_B T}\right]}{\exp\left[-\frac{h v_{^{52}Cr^{16}O}}{2k_B T}\right]} \right) \text{(S12)}$$

Where v is the vibrational frequency of the ^{53}Cr-^{16}O and ^{52}Cr-^{16}O bonds, h is Planck's constant, k_B is Boltzmann's constant and T is the absolute temperature. The vibrational frequency of the Cr-O bond for the abundance of natural Cr (molar mass 0.051996 kg/mol) is 864 cm^{-1} (45). Applying the formula for a single harmonic vibration;

$$v = \frac{1}{2\pi}\sqrt{k_s\left(\frac{1}{m_{Cr}} - \frac{1}{m_O}\right)} \text{ (S13)}$$

which yields, v^{52}Cr-^{16}O and v^{53}Cr-^{16}O, 864.0 cm^{-1} and 862.1 cm^{-1}, respectively. This gives:

$$10^3 \ln {}^{53/52}Cr\beta_{CrO} = 0.28 \times \frac{10^6}{T^2}. \text{ (S14)}$$

In order to calculate the more complex molecules CrO_2(g) (bent at 130° with C_{2v} symmetry) and CrO_3(g) (trigonal at 115° with C_{3v} symmetry) bond valence theory coupled with Born-Landé potentials were used. In the harmonic approximation (3), the β factor for a given phase (i) and isotope ratio (n/d) may be related to the sum of all force constants in a bonding environment (K_f) by a constant f that describes the quantum component of the partition function ratio, and is dependent on the relative mass difference between the two isotopes, and the absolute temperature (T):

$$10^3 \ln {}^{n/d}\beta_i = f\frac{K_f}{T^2}. \text{ (S15)}$$

The value of f is given by (see (3, 46)):

$$f = \frac{3N_A 10^3}{96\pi^2}\left(\frac{h}{k_B T}\right)^2\left(\frac{1}{m_n} - \frac{1}{m_d}\right), \text{ (S16)}$$

where N_A is Avogadro's number, h is Planck's constant, k_B Boltzmann's constant, m the molar mass. For the ^{53}Cr/^{52}Cr ratio, f = 1594. Though model-dependent, β factors calculated in this manner are rather accurate with respect to NRIXS measurements of force constants (*e.g.* 47). Here K_f, is estimated by approximating the bonds between Cr-O as ionic, and hence applying Born-Landé potentials (48, 49):

$$K_f = \frac{1}{4\pi\varepsilon_o}\frac{z_{Cr} z_O q^2 (B-1)}{r_{Cr-O}^3}. \text{ (S17)}$$

Here, ε_o is the permittivity of free space, z the formal charge, q the charge on an electron in coulombs, B the Born exponent and r the radius in metres. In order to match the calculation for Cr-O presented above, B was fixed at a value of 1.8 for gases and 2.7 for solids.

The results are shown in Table S12, and are in excellent accord. For example, the $10^3\ln\beta$ value for $^{53}Cr/^{52}Cr$ in Cr_2SiO_4 at 1000 K calculated in ref. (33) is 0.30, compared to 0.29 herein; likewise for Cr_2O_3, 0.53 *vs.* 0.50 herein. As a result, both the fractionation factor between solid and gas, and the absolute values of the solids have been benchmarked against DFT calculations, lending credence to the values calculated for Cr-bearing species herein. The variation of the $^{53}Cr/^{52}Cr$ $10^3\ln\beta$ factor for these species is summarised as a function of temperature in Figure S3.

Table S12. Input parameters and force constants of bond valence modelling.

Species	z_M	z_O	$r_{Cr\text{-}O\ (m)}$	$K_{f\ Cr\text{-}O}$	$10^3\ln\beta$ ($\times10^6/T^2$)	Reference#
$CrO_{(g)}$	2	2	1.62×10^{-10}	173.3	0.28	(45)
$CrO_{2(g)}$	4	2	1.60×10^{-10}	359.2	0.57	(45)
$CrO_{3(g)}$	6	2	1.58×10^{-10}	558.4	0.89	(45)
$Cr_2SiO_{4(s)}$	2	2	2.05×10^{-10}	182.5	0.29	(50)
$Cr_2O_{3(s)}$	3	2	1.96×10^{-10}	313.1	0.50	(51)

#values for bond lengths

The hierarchy of partitioning of heavy isotopes into Cr-bearing phases decreases in the order: $CrO_{3(g)}$ > $CrO_{2(g)}$ > $Cr_2O_{3(s)}$ > $Cr_2SiO_{4(s)}$ ≈ $CrO_{(g)}$ > $Cr^0_{(g)}$.

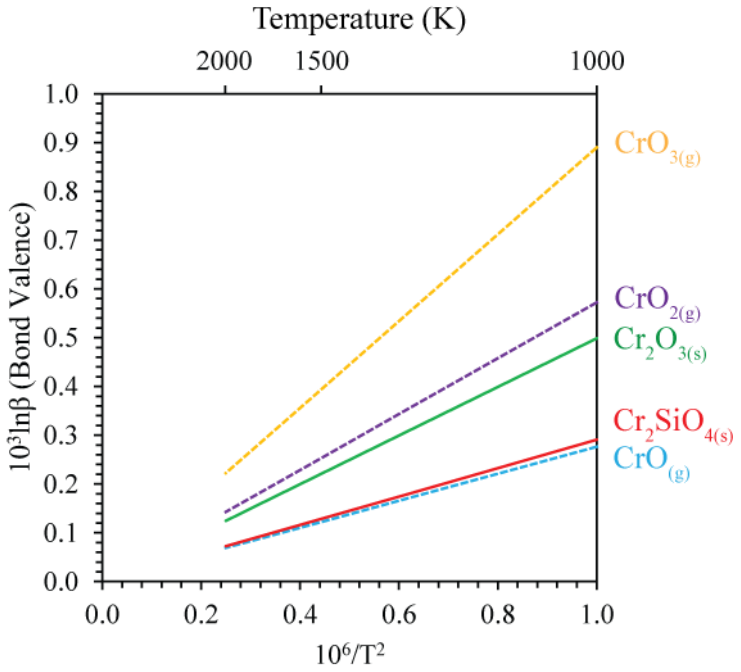

Figure S3. The $^{53}Cr/^{52}Cr$ $10^3\ln\beta$ factors calculated by the bond valence method (this work) for gases (dashed lines) and solids (solid lines) as a function of inverse temperature (K) squared.

References

1. Nisbet EG, Cheadle MJ, Arndt NT, Bickle MJ (1993) Constraining the potential temperature of the Archaean mantle : A review of the evidence from komatiites. *Lithos* 30:291–307.

2. Green DH, Nicholls IA, Viljoen MJ, Viljoen RP (1975) Experimental Demonstration of the Existence of Peridotitic Liquids in Earliest Archean Magmatism. *Geology* 3:11–14.

3. Urey HC (1947) The thermodynamic properties of isotopic substances. *J Chem Soc*:562–581.

4. Sossi PA, et al. (2016) Petrogenesis and Geochemistry of Archean Komatiites. *J Petrol* 57(1):147–184.

5. Sossi PA, Nebel O, O'Neill HSC, Moynier F (2018) Zinc isotope composition of the Earth and its behaviour during planetary accretion. *Chem Geol* 477:73–84.

6. Badullovich N, Moynier F, Creech J, Teng F, Sossi PA (2017) Tin isotopic fractionation during igneous differentiation and Earth's mantle composition. *Geochemical Perspect Lett* 5:24–28.

7. Gall L, Williams HM, Halliday AN, Kerr AC (2017) Nickel isotope composition of the mantle. *Geochim Cosmochim Acta* 1999:196–209.

8. Dauphas N, Teng F-Z, Arndt NT (2010) Magnesium and iron isotopes in 2.7 Ga Alexo komatiites: Mantle signatures, no evidence for Soret diffusion, and identification of diffusive transport in zoned olivine. *Geochim Cosmochim Acta* 74(11):3274–3291.

9. Delano JW (2001) Redox history of the Earth's interior since approximately 3900 Ma: implications for prebiotic molecules. *Orig Life Evol Biosph* 31(4-5):311–41.

10. Donaldson CH (1976) An experimental investigation of olivine morphology. *Contrib to Mineral Petrol* 57(2):187–213.

11. Faure F, Arndt NT, Libourel G (2006) Formation of Spinifex Texture in Komatiites: an Experimental Study. *J Petrol* 47(8):1591–1610.

12. Sossi PA, O'Neill HSC (2016) Liquidus temperatures of komatiites and the effect of cooling rate on element partitioning between olivine and komatiitic melt. *Contrib Mineral Petrol* 171(5):1–25.

13. Pyke DR, Naldrett AJ, Eckstrand OR (1973) Archean Ultramafic Flows in Munro Township, Ontario. *Geol Soc Am Bull* 84(3):955–978.

14. Tomlinson KY, et al. (1998) The Red Lake greenstone belt, Superior Province: evidence of plume-related magmatism at 3 Ga and evidence of an older enriched source. *Precambrian Res*

89:59–76.

15. Wieczorek M a. (2006) The Constitution and Structure of the Lunar Interior. *Rev Mineral Geochemistry* 60(1):221–364.

16. Walker D, Longhi J, Hays JF (1976) Heterogeneity in titaniferous lunar basalts. *Earth Planet Sci Lett* 30(1):27–36.

17. Poitrasson F, Halliday AN, Lee D, Levasseur S, Teutsch N (2004) Iron isotope differences between Earth , Moon , Mars and Vesta as possible records of contrasted accretion mechanisms. 223:253–266.

18. Wang K, Jacobsen SB, Sedaghatpour F, Chen H, Korotev RL (2015) The earliest Lunar Magma Ocean differentiation recorded in Fe isotopes. *Earth Planet Sci Lett* 430:202–208.

19. Sossi PA, Moynier F (2017) Chemical and isotopic kinship of iron in the Earth and Moon deduced from the lunar Mg-Suite. *Earth Planet Sci Lett* 471:125–135.

20. McCallum IS, Schwartz JM (2001) Lunar Mg suite: Thermobarometry and petrogenesis of parental magmas. *J Geophys Res* 106(E11):27969.

21. Shearer CK, Elardo SM, Petro NE, Borg LE, McCubin FM (2015) Origin of the lunar highlands Mg-suite: An integrated petrology, geochemistry, chronology, and remote sensing perspective. *Am Mineral* 100(1):294–325.

22. Norman MD, Ryder G (1980) Geochemical constraints on the igneous evolution of the lunar crust. *Proc. Lunar and Planetary Science Conference, 11th* (Lunar and Planetary Science Institute, Houston), pp 317–331.

23. Hess PC (1994) Petrogenesis of lunar troctolites. *J Geophys Res* 99:19083–19093.

24. Wänke H, Dreibus G, Palme H (1978) Primary matter in the lunar highlands: The case of the siderophile elements. *Proc. Lunar Planet. Sci. Conf. 9th*, pp 83–110.

25. Wasson JT, Boynton WV, Kallemeyn GW, Sundberg LL, Wai CM (1976) Volatile compounds released during lunar lava fountaining. *Proc Lunar Planet Sci Conf 7th*:1583–1595.

26. Delano JW (1986) Abundances of cobalt, nickel, and volatiles in the silicate portion of the moon. *Origin of the Moon* (Lunar and Planetary Science Institute, Houston), pp 231–247.

27. Dymek RF, Albee AL, Chodos AA (1975) Comparative petrology of lunar cumulate rocks of possible primary origin: Dunite 72415, troctolite 76535, norite 78235, and anorthosite 62237. *Proc Lunar Planet Sci Conf 6th*:301–341.

28. Ryder G, Bower JF (1977) Petrology of Apollo 15 black-and-white rocks 15445 and 15455 -

Fragments of the Imbrium impact melt sheet? *Lunar and Planetary Science Conference, 8th*, pp 1895–1923.

29. Berry AJ, O'Neill HSC, Scott DR, Foran GJ, Shelley JMG (2006) The effect of composition on Cr^{2+}/Cr^{3+} in silicate melts. *Am Mineral* 91(11-12):1901–1908.

30. Toplis MJ (2005) The thermodynamics of iron and magnesium partitioning between olivine and liquid: criteria for assessing and predicting equilibrium in natural and experimental systems. *Contrib to Mineral Petrol* 149(1):22–39.

31. Hanson B, Jones JH (1998) The systematics of Cr^{3+} and Cr^{2+} partitioning between olivine and liquid in the presence of spinel. *Am Mineral* 83:669–684.

32. Barnes SJ (1986) The distribution of chromium among orthopyroxene, spinel and silicate liquid at atmospheric pressure. *Geochim Cosmochim Acta* 50(9):1889–1909.

33. Moynier F, Yin Q-Z, Schauble E (2011) Isotopic evidence of Cr partitioning into Earth's core. *Science* 331(6023):1417–20.

34. Schoenberg R, Zink S, Staubwasser M, von Blanckenburg F (2008) The stable Cr isotope inventory of solid Earth reservoirs determined by double spike MC-ICP-MS. *Chem Geol* 249(3-4):294–306.

35. Schoenberg R, et al. (2016) The stable Cr isotopic compositions of chondrites and silicate planetary reservoirs. *Geochim Cosmochim Acta* 183:14–30.

36. Bonnand P, Parkinson IJ, Anand M (2016) Mass dependent fractionation of stable chromium isotopes in mare basalts: Implications for the formation and the differentiation of the Moon. *Geochim Cosmochim Acta* 175:208–221.

37. Keil K, Prinz M, Bunch TE (1971) Mineralogy, petrology, and chemistry of some Apollo 12 samples. *Proceedings of the Second Lunar Science Conference* (Lunar and Planetary Science Institute, Houston), pp 319–341.

38. Champness PE, Lorimer GW (1971) An electron microscopic study of a lunar pyroxene. *Contrib Mineral Petrol* 33(3):171–83.

39. Bence AE, Papike JJ (1972) Pyroxenes as recorders of lunar basalt petrogenesis: Chemical trends due to crystal-liquid interaction. *Proc Third Lunar Sci Conf* 1:431–469.

40. Walker D, et al. (1977) Slowly cooled microgabbros 15555 and 15065. *Proc. Lunar and Planetary Science Conference, 8th* (Lunar and Planetary Science Institute, Houston), pp 1521–1547.

41. French BM, Walter LS, Heinrich KJF (1970) Quantitative mineralogy of an Apollo 11 lunar sample. *Proceedings of the Apollo 11 Lunar Science Conference* (Lunar and Planetary Science Institute, Houston), pp 433–444.

42. Beaty DW, Albee AL (1978) Comparative petrology and possible genetic relations among the Apollo 11 basalts. *Proc. Lunar and Planetary Science Conference, 9th* (Lunar and Planetary Science Institute, Houston), p 359–463.

43. Chase MW (1998) NIST-JANAF Thermochemical Tables, 4th Ed. J. Phys. Chem. Ref. Data. 1998, Monograph 9(Part I and Part II). *J Phys Chem Ref Data* Monograph:Part I&II.

44. Schauble EA (2004) Applying Stable Isotope Fractionation Theory to New Systems. *Reviews in Mineralogy and Geochemistry: Geochemistry of Non-Traditional Stable Isotopes*, eds Johnson CM, Beard BL, Albaréde F (Mineralogical Society of America, Washington DC), pp 65–111. 55th Ed.

45. Espelid O, Borve KJ, Jensen VR (1998) Structure and thermodynamics of gaseous oxides, hydroxides, and mixed oxohydroxides of chromium: $CrO_m(OH)_{(n)}$ (m, n = 0-2) and CrO_3. A computational study. *J Phys Chem A* 102(50):10414–10423.

46. Young ED, Galy A, Nagahara H (2002) Kinetic and equilibrium mass-dependent isotope fractionation laws in nature and their geochemical and cosmochemical significance. *Geochim Cosmochim Acta* 66(6):1095–1104.

47. Blanchard M, et al. (2009) Iron isotope fractionation between pyrite (FeS_2), hematite (Fe_2O_3) and siderite ($FeCO_3$): A first-principles density functional theory study. *Geochim Cosmochim Acta* 73(21):6565–6578.

48. Born M, Mayer JE (1932) Zur Gittertheorie der ionenkristalle. *Zeitschrift fur Phys* 75(1):1–18.

49. Young ED, Tonui E, Manning CE, Schauble EA, Macris CA (2009) Spinel–olivine magnesium isotope thermometry in the mantle and implications for the Mg isotopic composition of Earth. *Earth Planet Sci Lett* 288:524–533.

50. Dollase WA, Seifert F, O'Neill HSC (1994) Structure of Cr_2SiO_4 and possible metal-metal interactions in crystal and melt. *Phys Chem Miner* 21(1):104–109.

51. Finger LW, Hazen RM (1980) Crystal structure and isothermal compression of Fe_2O_3, Cr_2O_3, and V_2O_3 to 50 kbars. *J Appl Phys* 51(10):5362–5367.